# Monotone Switches in Implicit Algorithms for Potential Equations Applied to Transonic Flows

Peter M. Goorjian*
*NASA Ames Research Center, Moffett Field, California*
and
Michael E. Meagher† and Robert Van Buskirk‡
*Informatics General Corporation, Palo Alto, California*

**Numerical calculations of transonic flows by potential equations typically use algorithms that change the method of calculation for regions of subsonic and supersonic flow. In this paper, implicit approximate-factorization algorithms are modified to use the monotonic switch in the type of finite differencing that was developed by Godunov for the Euler equations. Calculations of flows over airfoils by these algorithms are compared with calculations by other commonly used methods. For the small-disturbance potential equation, comparisons are made with the Murman-Cole method for both steady and unsteady flows. For the full potential equation, comparisons are made with the method of Holst and Ballhaus for steady flows. The comparisons show that the monotone methods are more stable. For steady flows, converged solutions are obtained for cases where the older methods fail. For unsteady flows, solutions are obtained for cases where the Murman-Cole switch requires a time step more than ten times smaller in order for the calculations to remain stable. These improvements are achieved with no increase in computer storage and only minor modifications in current codes.**

## I. Introduction

THE treatment of shock waves and sonic lines is a central issue in the computation of transonic flows. Calculations of transonic flows in two dimensions by potential equations typically use algorithms that change methods across such lines. In this paper, implicit approximate-factorization algorithms are modified to use the monotonic switch developed by Godunov. Calculations of flows over airfoils by these monotone algorithms are compared with calculations by nonmonotone methods. The comparisons show that the monotone switches improve the algorithms by making the calculations stable for cases that were unstable when nonmonotone switches were used.

In Ref. 1, the definition of monotonicity is given for explicit finite difference schemes. We call an implicit scheme monotone if the reduction of that scheme to an explicit one results in a monotone scheme.

### Small-Disturbance Potential Equations

Most of the algorithms in transonic small-disturbance potential codes use the Murman-Cole[2] method of changing the type of calculations for regions of supersonic and subsonic flow. For example, in finite difference methods, central differencing is used in subsonic regions of the flow and upwind differencing is used in supersonic regions. This change of the algorithm takes into account the fundamentally different character of the subsonic and supersonic regions in transonic flowfields. A weakness in this method is that it allows stable solutions of which the flowfield contains entropy violating expansion shocks[3] in one-dimensional model cases. In comparison, monotone methods do not allow these nonphysical solutions.[1] In two-dimensional flows over an airfoil, we will show that this weakness in the Murman-Cole method will allow numerical instabilities to develop in the calculations near the leading edge of the airfoil. However, the results from the monotonic methods display no such instabilities.

The description of the new algorithms and the computations for the small-disturbance equation are presented in Secs. II and III. In those sections, implicit approximate-factorization algorithms[4,5] are modified to implement the monotone switch developed by Godunov.[6,7] In Ref. 8, a detailed comparison is made of the Murman-Cole[2] and Godunov methods of switching the type-dependent differencing, as well as the Enquist-Osher[9,10] monotone switch. Also in Ref. 8 are sections on one-dimensional algorithms that form the basis of the two-dimensional algorithms presented in this article. Sample one-dimensional calculations in Ref. 8 clearly demonstrate the deficiency at sonic expansion points for the nonmonotone switches.

### Full Potential Equation

Most of the algorithms in transonic full-potential codes use type-dependent differencing that is a generalization of the Murman-Cole method. Examples are the artificial viscosity method of Jameson[11] and a variant of that method developed by Holst and Ballhaus[12] that uses an upwind bias of the density. These nonmonotone methods suffer from a weakness similar to that of the Murman-Cole method in dealing with nonphysical expansion shocks.[8] This deficiency causes numerical instabilities in two-dimensional calculations.

In Ref. 8, a sample calculation in one dimension shows that the use of a monotone switch forcefully smooths out an initial expansion shock, whereas the methods of Jameson and of Holst and Ballhaus only weakly suppress it. In Sec. IV, a monotone switch is implemented in an implicit approximate-factorization algorithm[12] for flow in two dimensions. This monotone algorithm uses type-dependent differencing in the streamwise direction in the manner of the rotated differencing scheme of Jameson.[11] A sample calculation shows that the monotone algorithm produces a converged solution for a flow for which the nonmonotone algorithm called AF2, of Holst and Ballhaus,[12] is unstable. The monotone results were obtained by making only minor modifications to a code that uses the AF2 algorithm.

Received Dec. 13, 1982; presented as Paper 83-0371 at the AIAA 21st Aerospace Sciences Meeting, Reno, Nev., Jan. 10-13, 1983; revision received May 15, 1984. This paper is declared a work of the U.S. Government and therefore is in the public domain.

*Research Scientist. Member AIAA.
†Analyst; also Student, University of California, Santa Cruz.
‡Analyst; also Student, University of California, Berkeley.

## II. Two-Dimensional Steady Algorithm for the Small-Disturbance Equation

In this section we shall present an algorithm for solving the transonic, small-disturbance potential equation in two dimensions for steady flows that uses the Godunov switch.[6,7] That switch is based on using solutions to the Riemann problem with initial values that model the flow in a shock tube.[13] Reference 7 illustrates in detail the selection of the numerical flux function that is used in the Godunov switch. Two comparisons of its computed results with those from an algorithm using the Murman-Cole switch[4] are then made. For the first comparison the methods behave similarly; however, in the second case the monotone switch produces a converged solution, whereas the old method is unstable. The source of this instability is displayed in the unsteady calculations shown in Sec. III.

### Governing Equation

An algorithm is presented for the low-frequency, unsteady, small-disturbance potential equation

$$2kM_\infty^2\phi_{xt} = [(1-M_\infty^2) - (\gamma+1)M_\infty^m\phi_x]\phi_{xx} + \phi_{yy} \qquad (1)$$

where $k$ is the reduced frequency; $M_\infty$ the freestream Mach number; $x$ and $y$ the freestream and stream-normal coordinate directions, respectively; $\gamma$ the ratio of specific heats, $\gamma = 1.4$ for air; and $m$ is a function[5] of $M_\infty$ that adjusts the critical pressure coefficient $C_p^*$ for Eq. (1) to match that exact isentropic $C_p^*$. Although Eq. (1) is physically meaningful for unsteady flows,[5,14] the algorithms considered in this section are nonconservative in time and therefore are only useful for calculations of steady flows. However, by being nonconservative in time, a nonlinear instability in the shock motion is eliminated,[8,14] and the steady calculations become more efficient.

### Algorithm

An approximate-factorization implicit algorithm called AF2, which uses the Murman-Cole[4,14] switch is modified. Since our modification uses the monotone switch of Godunov, we call it MAF-G. It is given by the following two-step finite difference approximation to Eq. (1) at mesh point $(i,j)$.

Step 1:

$$[\alpha - (A_{i,j}D_x)]f_{i,j} = [\alpha^2\overleftarrow{\delta}_x + (A_{i,j}D_x)\delta_{yy}]\phi_{i,j}^n + \alpha(\omega-1)R_{i,j}^n \qquad (2)$$

Step 2:

$$(\alpha\overleftarrow{\delta}_x - \delta_{yy})\phi_{i,j}^{n+1} = f_{i,j}^n$$

where

$$A_{i,j}D_x = \tilde{G}_{i,j}\vec{\Delta}_x + \hat{G}_{i,j}\overleftarrow{\Delta}_x$$

$$\tilde{G}_{i,j} = (1-\epsilon_{i,j})(\tilde{A}_{i+\frac{1}{2},j} + \hat{A}_{i-\frac{1}{2},j}) + \tilde{A}_{i-\frac{1}{2},j}$$

$$\hat{G}_{i,j} = \epsilon_{i-1,j}(\tilde{A}_{i-\frac{1}{2},j} + \hat{A}_{i-(3/2),j}) + \hat{A}_{i-\frac{1}{2},j}$$

$$\tilde{A}_{i-\frac{1}{2},j} = \tfrac{1}{2}C_1 + C_2\tilde{u}_{i-\frac{1}{2},j}^n$$

$$\hat{A}_{i-\frac{1}{2},j} = \tfrac{1}{2}C_1 + C_2\hat{u}_{i-\frac{1}{2},j}^n$$

$$\tilde{u}_{i-\frac{1}{2},j}^n = \bar{u} + (1-\epsilon_{i-\frac{1}{2},j})(u_{i-\frac{1}{2},j}^n - \bar{u})$$

$$\hat{u}_{i-\frac{1}{2},j} = \bar{u} + \epsilon_{i-\frac{1}{2},j}(u_{i-\frac{1}{2},j}^n - \bar{u})$$

$$C_1 = 1 - M_\infty^2$$

$$C_2 = -\tfrac{1}{2}(\gamma+1)M_\infty^m$$

$$\bar{u} = -C_1/2C_2$$

$$\epsilon_{i-\frac{1}{2},j} = 0 \quad \text{if } u_{i+\frac{1}{2},j} \le \bar{u} \quad \text{(subsonic)}$$

$$= 1 \quad \text{otherwise} \quad \text{(supersonic)}$$

$$\epsilon_{i,j} = 0 \quad \text{if } u_{i+\frac{1}{2},j} + u_{i-\frac{1}{2},j} \le 2\bar{u}$$

(possible upstream moving shock)

$$= 1 \quad \text{otherwise}$$

(possible downstream moving shock)

$$u_{i-\frac{1}{2},j}^n = \overleftarrow{\delta}_x\phi_{i,j}^n = \frac{\phi_{i,j}^n - \phi_{i-1,j}^n}{x_i - x_{i-1}}$$

$$\vec{\Delta}_x f_{i,j}^n = \frac{f_{i+1,j}^n = f_{i,j}^n}{\frac{1}{2}(x_{i+1} - x_{i-1})}$$

$$\overleftarrow{\Delta}_x f_{i,j}^n = \frac{f_{i,j}^n - f_{i-1,j}^n}{\frac{1}{2}(x_{i+1} - x_{i-1})}$$

$$\alpha = 2kM_\infty^2/\Delta t$$

where $\omega$ is a relaxation parameter, $R^n$ is the residual given by

$$R_{i,j}^n = (A_{i,j}D_x\overleftarrow{\delta}_x + \delta_{yy})\phi_{i,j}^n$$

$\delta_{yy}$ is a central, second-difference operator in the $y$ direction and $\bar{u}$ is the sonic value of $\phi_x$. The Murman-Cole switch uses only the $\epsilon_{i,j}$ switch; see Refs. 4 and 8 for a comparison of the two algorithms. The special forms of $\overleftarrow{\Delta}_x$ and $\vec{\Delta}_x$ are chosen to maintain conservation form in a nonuniform mesh, which was used for the calculations. MAF-G is identical to AF2 except in the region where the flowfield changes type, which is near the sonic lines and shock waves.

Equation (2) is solved iteratively using $\phi^n$ to obtain $\phi^{n+1}$ until a converged solution is obtained. The term $\alpha$, which is inversely proportional to the time step size $\Delta t$, is used to calculate the convergence process and was chosen from a geometric sequence[4] of eight acceleration parameters, which start from a high value $\alpha_H$ and decrease to a low value $\alpha_L$. These parameters are cycled through repeatedly until a converged solution is obtained. The relaxation parameter $\omega$, where $0 \le \omega \le 2$, is also used to accelerate the convergence.

### Computed Results

A series of comparisons between results obtained using AF2 and MAF-G was made. The computations were made using the NASA Ames code[5] LTRAN2. This unsteady code uses the AF2 algorithm in a subroutine to compute steady flows for use as initial conditions for the unsteady calculations. By making only minor changes to that subroutine, the monotone switch was implemented. Hence, any difference in computed results is due solely to the differences in the switches.

Figure 1 shows a converged solution obtained by both the MAF-G and the AF2 methods. The flow is about a Korn airfoil at an angle of attack $\alpha = 0.5$ deg and $M_\infty = 0.75$. The two methods gave values of the pressure coefficients that were identical to within plottable accuracy. Note that the results show the postshock re-expansion singularity. Also, only one mesh point value occurs within the shock wave. For both methods the values $\omega = 1.9$, $\alpha_L = 5.4$, and $\alpha_H = 225$ were used. These values were determined by finding the optimum convergence rate for each switch for flow over a 10% thick parabolic arc airfoil at $M_\infty = 0.87$ and $\alpha = 0$ deg. Both methods had the same optimal values. Convergence was obtained by reducing the maximum residual by four orders of magnitude.

The next calculation is the flow about a NACA 64A006 airfoil at $M_\infty = 0.8$ and $\alpha = 2$ deg. Figure 2 shows the converged solution obtained by the MAF-G method. The AF2 method

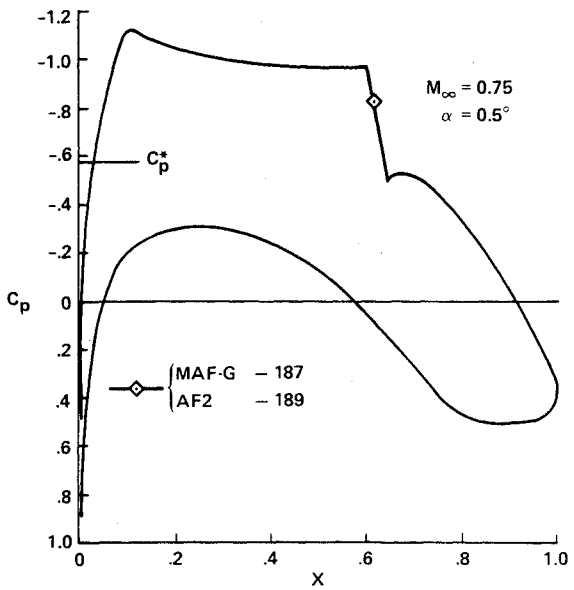


**Fig. 1 Converged solution obtained using MAF-G and AF2. Pressure coefficients plot for Korn airfoil at $\alpha = 0.5$ deg, $M_\infty = 0.75$.**

diverged in this case in 138 iterations. This divergence is due to the growth of a numerical instability that is allowed by the defective sonic point operator of the Murman-Cole switch. The instability starts at the leading edge of the airfoil and will be illustrated in the unsteady calculation shown in Sec. III. For the calculations shown in Fig. 2, the values $\omega = 1.0$, $\alpha_L = 5$, and $\alpha_H = 700$ were used. Converged solutions were also obtained using $\alpha_H = 500$ and 900. AF2 diverged in all these cases.

In addition to the two cases shown in Figs. 1 and 2, flows were computed about a 10% thick parabolic arc airfoil with $\alpha = 0$ deg and $M_\infty = 0.85$, 0.87, and 0.9. In the latter case, there is a fishtail shock-wave pattern formed in the flow. For these cases, the AF2 calculations were stable and both methods converged in approximately the same number of iterations.

#### Conclusions

By slightly modifying the AF2 algorithm to implement the Godunov switch, a more stable algorithm is obtained, while retaining the accuracy and speed of the AF2 algorithm as shown in Fig. 1.

## III. Two-Dimensional Unsteady Algorithm for the Small-Disturbance Equation

In this section an algorithm for solving Eq. (1) is presented. This algorithm will be conservative in both time and space and will therefore correctly simulate unsteady transonic flows. Comparisons will be made between the computer code[5] LTRAN2, with the Murman-Cole switch, and this new monotone code, called LTRAN2-MG. For the case considered, LTRAN2 requires significantly smaller time-step sizes than LTRAN2-MG for the calculations to remain stable. Also, the source of the numerical instability in the LTRAN2 calculations will be illustrated in the plots of the pressure coefficients.

#### Algorithm

The alternating direction implicit (ADI) algorithm[5] used in LTRAN2 is modified. This modified algorithm is given by the following two-step finite difference procedure to advance the solution from time level $n$ to time level $n+1$ at mesh point $(i,j)$.

$x$-sweep

$$\alpha\delta_x(\phi^*_{i,j} - \phi^n_{i,j}) = \bar{D}_x f_{i-\frac{1}{2},j} + \delta_{yy}\phi^n_{i,j} \tag{3}$$

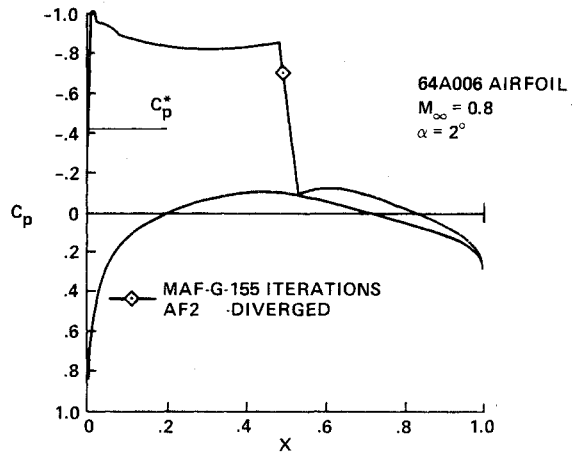


**Fig. 2 Converged solution obtained using the MAF-G algorithm. Pressure coefficients plot for the 64A006 airfoil at $\alpha = 2$ deg and $M_\infty = 0.8$.**

$y$-sweep

$$\alpha\delta_x(\phi^{n+1}_{i,j} - \phi^*_{i,j}) = \tfrac{1}{2}\delta_{yy}(\phi^{n+1}_{i,j} - \phi^n_{i,j})$$

where

$$\bar{D}_x f_{i-\frac{1}{2},j} = \vec{\Delta}_x \tilde{f}_{i-\frac{1}{2},j} + \overleftarrow{\Delta}\hat{f}_{i-\frac{1}{2},j}$$

$$\tilde{f}_{i-\frac{1}{2},j} = \tfrac{1}{2}[C_1\tilde{u}_{i-\frac{1}{2},j} + (C_1 + 2C_2\tilde{u}_{i-\frac{1}{2},j})\overleftarrow{\delta}_x\phi^*_{i,j}]$$

$$\hat{f}_{i-\frac{1}{2},j} = \tfrac{1}{2}[C_1\hat{u}_{i-\frac{1}{2},j} + (C_1 + 2C_2\hat{u}_{i-\frac{1}{2},j})\overleftarrow{\delta}_x\phi^*_{i,j}]$$

$$\vec{\Delta}_x\tilde{f}_{i-\frac{1}{2},j} = \frac{\tilde{f}_{i+\frac{1}{2},j} - \tilde{f}_{i-\frac{1}{2},j}}{\frac{1}{2}(x_{i+1} - x_{i-1})}$$

$$\overleftarrow{\Delta}_x\hat{f}_{i-\frac{1}{2},j} = \frac{\hat{f}_{i-\frac{1}{2},j} - \hat{f}_{i-3/2,j}}{\frac{1}{2}(x_{i+1} - x_{i-1})}$$

$$\delta_x\phi^n_{i,j} = \frac{\phi^n_{i,j} - \phi^n_{i-1,j}}{\frac{1}{2}(x_{i+1} - x_{i-1})}$$

In this section

$$\tilde{u}_{i+\frac{1}{2},j} = \bar{u} + (1 - \epsilon_{i,j})(1 - \epsilon_{i+\frac{1}{2},j})(u^n_{i+\frac{1}{2},j} - \bar{u})$$

$$\hat{u}_{i-\frac{1}{2},j} = \bar{u} + \epsilon_{i,j}\epsilon_{i-\frac{1}{2},j}(u^n_{i-\frac{1}{2},j} - \bar{u})$$

Finally, $\alpha$, $\delta_{yy}$, $C_1$, $C_2$, $\bar{u}$, and $\overleftarrow{\delta}_x\phi^n_{i,j}$ are defined in the same way as in Sec. II. As in Sec. II, the special forms of $\overleftarrow{\Delta}_x$, $\vec{\Delta}_x$, and $\delta_x$ are used to maintain conservation form in a nonuniform mesh. See Refs. 5 and 8 for a comparison with the Murman-Cole switch. The actual coding of the Godunov switch only required a minor modification in the code LTRAN2.

#### Computed Results

The computed flow is about a NACA 64A010 airfoil in pitching motion about the quarter-chord point with unsteady angle of attack $\alpha = 1$ deg $\sin(kt)$, $k = 0.05$, $M_\infty = 0.80$, and $k\Delta t = 3$ deg. The airfoil ordinates used were taken from the experimental model reported in Ref. 15. Figure 3 shows comparisons of upper surface-pressure coefficients at two times computed by LTRAN2-MG and LTRAN2. The jaggedness in the pressure-coefficient profile of LTRAN2-MG near the leading edge is due to the use of the experimental airfoil ordinates. Although there is a shock wave located near the midchord, Fig. 3a shows that it is not the source of the numerical instability in the calculations using LTRAN2. In Fig. 3a the flow is advanced to the time when the instabilities in LTRAN2

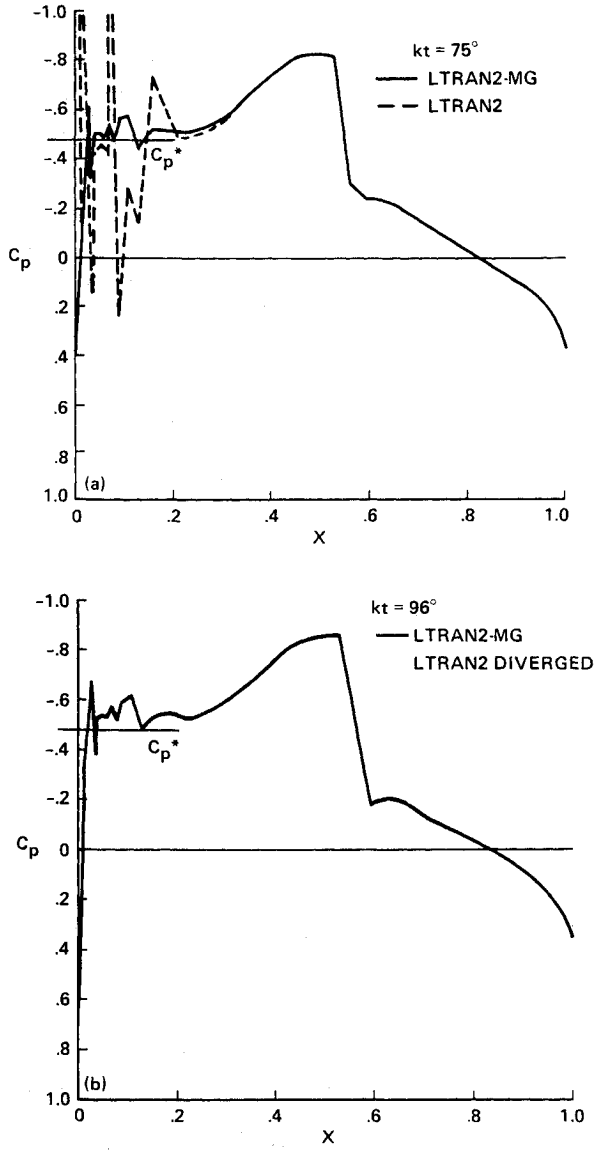


**Fig. 3 Comparison of LTRAN2 and LTRAN2-MG. Upper surface-pressure coefficient plots of an NACA 64A010 airfoil (experimental ordinates from Ref. 15) in pitching motion with $\alpha = 1$ deg sin($kt$) about the quarter chord point with a reduced frequency $k = 0.05$ and $M_\infty = 0.80$. a) $kt = 75$ deg; b) $kt = 96$ deg, LTRAN2 has diverged but LTRAN2-MG is stable.**

start occurring. By this time the shock wave at the midchord has strengthened and the jagged profile near the leading edge repeatedly crosses the sonic value with spike-like structures. These spikes in the flow place sonic- and shock-point operators near each other and it is in this region that the Murman-Cole switch becomes unstable. A short time later, as shown in Fig. 3b, the LTRAN2 calculation has diverged. In comparison, the LTRAN2-MG calculation continues to evolve the flow in a stable fashion, including the fine spike-like structures at the leading edge. In order to stabilize the calculations using LTRAN2, the time-step size had to be reduced to $k\Delta t = 0.25$ deg, which is 12 times smaller than the time step used with LTRAN2-MG. With the smaller time step, the LTRAN2 calculations agreed with those from LTRAN2-MG.

Additional comparisons were made between LTRAN2 and LTRAN2-MG for flow over an NACA 64A006 airfoil, using the theoretical airfoil ordinates. The airfoil was in plunging motion for $M_\infty = 0.8$ and 0.85 with $\alpha = 0$ deg and for $M_\infty = 0.8$ with $\alpha = 1$ deg. In all these additional cases the LTRAN2 code had to use a time-step size that was approximately 10 times smaller than that for LTRAN2-MG in order to reproduce the stable calculation of the monotone code. In all these cases, the instability in the LTRAN2 calculations using the larger time steps started at the leading edge of the airfoil. The pressure coefficient plots displayed a single spike or oscillatory structure at the leading edge that crosses the sonic value. Hence, it must also be concluded in these cases that proximity of the sonic and shock point operators caused the calculations using the Murman-Cole switch to become unstable. In the first two cases, the calculations diverged. In the third case, the instabilities were transient, so that the calculations did not diverge but contained large errors. This situation can be more troublesome than a divergent calculation to code users such as aeroelasticians, since errors in such quantities as unsteady aerodynamic loads might go undetected.

#### Conclusions

By slightly modifying the LTRAN2 algorithm to implement the Godunov switch in place of the Murman-Cole switch, calculations using time steps ten times larger than before were possible.

## IV. Two-Dimensional Steady Algorithm for the Full Potential Equation

In this section, an implicit algorithm for the steady, full potential equation in two dimensions will be modified to implement the Godunov switch. The monotone switch will be implemented in the AF2 algorithm developed in Ref. 12. The type-dependent differencing will be performed in the streamwise direction by using the rotated, coordinate differencing scheme developed in Ref. 11. In Ref. 8, a monotone switch is developed for one-dimensional flows, which forms the basis for the switch developed in this section. Also in Ref. 8, a one-dimensional calculation clearly shows the weakness of the nonmonotone switches used in Refs. 10 and 11.

#### Governing Equation

The model governing equation is

$$\phi_{xt} = (\rho\phi_x)_x + (\rho\phi_y)_y \tag{4}$$

where the density $\rho$ and the potential $\phi$ are given by

$$\rho = \left[\frac{2}{(\gamma+1)}a^2\right]^{1/(\gamma-1)} \tag{5}$$

$$a^2 = \left(\frac{\gamma+1}{2}\right)\left[1-\left(\frac{\gamma-1}{\gamma+1}\right)q^2\right] \tag{6}$$

$$q^2 = u^2 + v^2 = \phi_x^2 + \phi_y^2$$

$q$ and $\rho$ have been nondimensionalized by the sonic sound speed $a^*$ and the stagnation density $\rho_s$, respectively.

#### Algorithm

The spatial differencing of the approximate factorization scheme 2 (AF2) developed in Ref. 12 is modified. Our monotone scheme, MAF, is given by the following two-step, finite difference approximation to Eq. (4) at mesh point $(i,j)$.

Step 1:

$$(\alpha\overleftarrow{\delta}_x - \overleftarrow{\delta}_y\rho_{i,j+\frac{1}{2}}\overrightarrow{\delta}_y)f^n_{i,j} = \alpha\omega R^n_{i,j} \tag{7}$$

Step 2:

$$(\alpha - \tilde{\rho}_{i+\frac{1}{2},j}\delta_x)C^n_{i,j} = f^n_{i,j} \tag{8}$$

where

$$C^n_{i,j} = \phi^{n+1}_{i,j} - \phi^n_{i,j}$$

$$\overleftarrow{\delta}_x f^n_{i,j} = (f^n_{i,j} - f^n_{i-1,j})/(x_i - x_{i-1})$$

$$\overrightarrow{\delta}_y f^n_{i,j} = (f^n_{i,j+1} - f^n_{i,j})/(y_{j+1} - y_j)$$

$R^n_{i,j}$ is the residual given by

$$R^n_{i,j} = (\overleftarrow{\delta}_x \tilde{\rho}_{i+\frac{1}{2},j}\delta_x + \overleftarrow{\delta}_y p_{i,j+\frac{1}{2}}\overrightarrow{\delta}_y)\phi^n_{i,j}$$

$$\rho_{i+\frac{1}{2},j} = \tfrac{1}{2}(\rho_{i+\frac{1}{2},j+\frac{1}{2}} + \rho_{i+\frac{1}{2},j-\frac{1}{2}})$$

$$\rho_{i,j+\frac{1}{2}} = \tfrac{1}{2}(\rho_{i+\frac{1}{2},j+\frac{1}{2}} + \rho_{i-\frac{1}{2},j+\frac{1}{2}})$$

$$\tilde{\rho}_{i+\frac{1}{2},j}\delta_x\phi^n_{i,j} = [\rho_{i+\frac{1}{2},j} - \tilde{\nu}_{i+\frac{1}{2},j}(\rho_{i+\frac{1}{2},j} - \rho^*)]\overrightarrow{\delta}_x\phi_{i,j} + [\hat{\nu}_{i-\frac{1}{2},j}(\rho_{i-\frac{1}{2},j} - \rho^*)]\overleftarrow{\delta}_x\phi_{i,j} \tag{9}$$

$$\rho_{i+\frac{1}{2},j+\frac{1}{2}} = \left[1 - \left(\frac{\gamma-1}{\gamma+1}\right)(u^2+v^2)^n_{i+\frac{1}{2},j+\frac{1}{2}}\right]^{1/(\gamma-1)}$$

$$u^n_{i+\frac{1}{2},j+\frac{1}{2}} = \tfrac{1}{2}\overrightarrow{\delta}_x(\phi^n_{i,j} + \phi^n_{i,j+1})$$

$$v^n_{i+\frac{1}{2},j+\frac{1}{2}} = \tfrac{1}{2}\overrightarrow{\delta}_y(\phi^n_{i,j} + \phi^n_{i+1,j})$$

$\rho^*$ is the sonic value of the density, $=0.6339138$,

$$\tilde{\nu}_{i+\frac{1}{2},j} = \left(1 - \frac{1}{\tilde{M}^2_{i+\frac{1}{2},j}}\right)(\tfrac{1}{2})\left(1 + \frac{q^*}{q_{i+\frac{1}{2},j}}\right)\text{CON}$$

$$\text{if } M_{i+\frac{1}{2},j} \geq 1 \quad \text{or} \quad M_{i,j} \geq 1$$

$$= 0 \quad \text{otherwise} \tag{10}$$

$$\hat{\nu}_{i-\frac{1}{2},j} = \tilde{\nu}_{i-\frac{1}{2},j} \text{ if } M_{i-\frac{1}{2},j} \geq 1 \text{ and } M_{i,j} \geq 1$$

$$= 0 \quad \text{otherwise} \tag{11}$$

$$M^2_{i+\frac{1}{2},j} = \left(\frac{q^2}{a^2}\right)^n_{i+\frac{1}{2},j}$$

$$M^2_{i,j} = \tfrac{1}{2}(M^2_{i+\frac{1}{2},j} + M^2_{i-\frac{1}{2},j})$$

$$\text{CON} = 1.5^*\tilde{M}_{i+\frac{1}{2},j}$$

$$\tilde{M}^2_{i+\frac{1}{2},j} = \tfrac{1}{2}(\tilde{M}^2_{i+\frac{1}{2},j+\frac{1}{2}} + \tilde{M}^2_{i+\frac{1}{2},j-\frac{1}{2}})$$

$$\tilde{M}_{i+\frac{1}{2},j+\frac{1}{2}} = \left(\frac{\tilde{q}^2}{\tilde{a}^2}\right)^n_{i+\frac{1}{2},j+\frac{1}{2}}$$

$$(q^2)^n_{i+\frac{1}{2},j+\frac{1}{2}} = \tfrac{1}{4}(q^* + q_{i+\frac{1}{2},j+\frac{1}{2}})^2$$

$$\tilde{a}^2 = \left(\frac{\gamma+1}{2}\right)\left[1 - \left(\frac{\gamma-1}{\gamma+1}\right)\tilde{q}^2\right] \tag{12}$$

$\alpha = 1/\Delta t$ is an acceleration parameter and $\omega$ a relaxation parameter, $=2.0$ for the calculations in this section.

Equations (7) and (8) are solved iteratively using $\phi^n_{i,j}$ to obtain $\phi^{n+1}_{i,j}$ until a converged solution is obtained. The acceleration parameter $\alpha$ was chosen from a geometric sequence[4,12] of eight values starting from a high value $\alpha_H$ and decreasing to a low value $\alpha_L$. These parameters are cycled through repeatedly until a converged solution is obtained. This monotone scheme uses central differencing and is second-order accurate in subsonic regions. In supersonic regions, the additional terms in Eq. (9) make the scheme first-order accurate.

For a comparison with AF2, see Refs. 8 and 12. Equations (7) and (8) are unchanged. For AF2, Eq. (9) is replaced by a flux that uses a nonmonotone switch, called upwind density biasing. That flux is given by

$$\tilde{\rho}_{i+\frac{1}{2},j}\delta_x\phi^n_{i,j} = [\rho_{i+\frac{1}{2},j} - \nu_{i,j}(\rho_{i+\frac{1}{2},j} - \rho_{i-\frac{1}{2},j})]\overrightarrow{\delta}_x\phi_{i,j} \tag{13}$$

$$\nu_{i,j} = (1 - 1/M^2_{i,j})\text{CON} \quad \text{if } M_{i,j} \geq 1 \text{ supersonic}$$

$$= 0 \quad \text{if } M_{i,j} < 1 \text{ subsonic}$$

$$\text{CON} = 1.5^*M^2_{i,j}$$

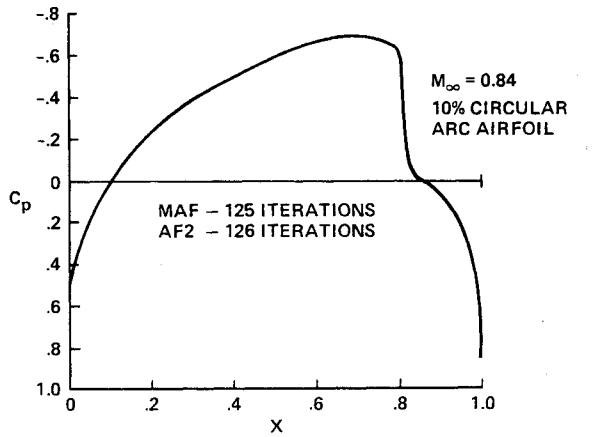


**Fig. 4 Circular-arc airfoil, 10% thick. Pressure coefficients. Sonic instability in AF2 passive. Converged solution using monotone (MAF) and nonmonotone (AF2) algorithms.**

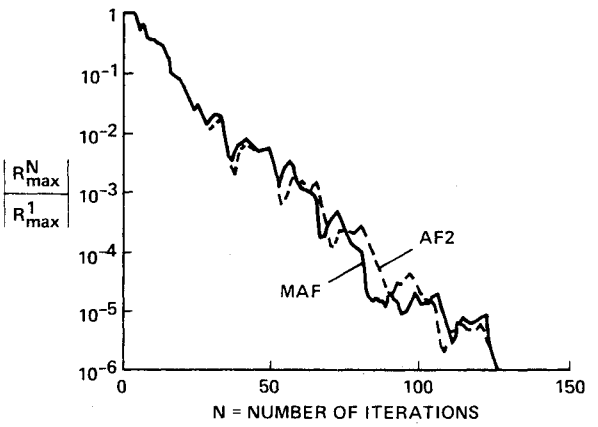


**Fig. 5 Maximum residual convergence history comparison between monotone (MAF) and nonmonotone (AF2) algorithms for case shown in Fig. 4.**

The essence of the difference between MAF and AF2 is seen by comparing Eqs. (9) and (13). Whereas Eq. (13) smoothly shifts the flow variables upwind as the flow becomes supersonic, Eq. (9) smoothly shifts the flow variables to sonic values and shifts flow variables located upwind away from sonic values. Both methods treat shock waves identically, but the monotone method is more stable at sonic expansion points.

### Computed Results

In this section, comparisons are made between MAF and AF2 for three computed flows. The calculations were made on a Cartesian mesh with variable spacing in the $x$ and $y$ coordinate directions. A $90 \times 21$ mesh was used with 47 points on the airfoil surface. The flows were nonlifting, so that only flow in the upper half plane was computed. Also, small-disturbance boundary conditions on the airfoil were used for these test cases. The boundaries were located five chord lengths away from the airfoil in the $x$ direction and six chord lengths away in the $y$ direction. The calculations were made by a nonlifting research code that implemented the AF2 algorithm. The MF calculations were made by only making minor modifications to the spatial differencing of the research code. Hence, any difference in the comparisons is due solely to the different switches.

The first comparison is of a flow over a 10% thick circular-arc airfoil at $M_\infty = 0.84$. Within plottable accuracy, Fig. 4 shows that the two methods give identical answers. For this case, the numerical instability in the AF2 switch that may occur at the sonic expansion line is not activated. Hence, the two methods obtained the converged solution at a similar rate, as shown in Fig. 5 by their maximum residual convergence

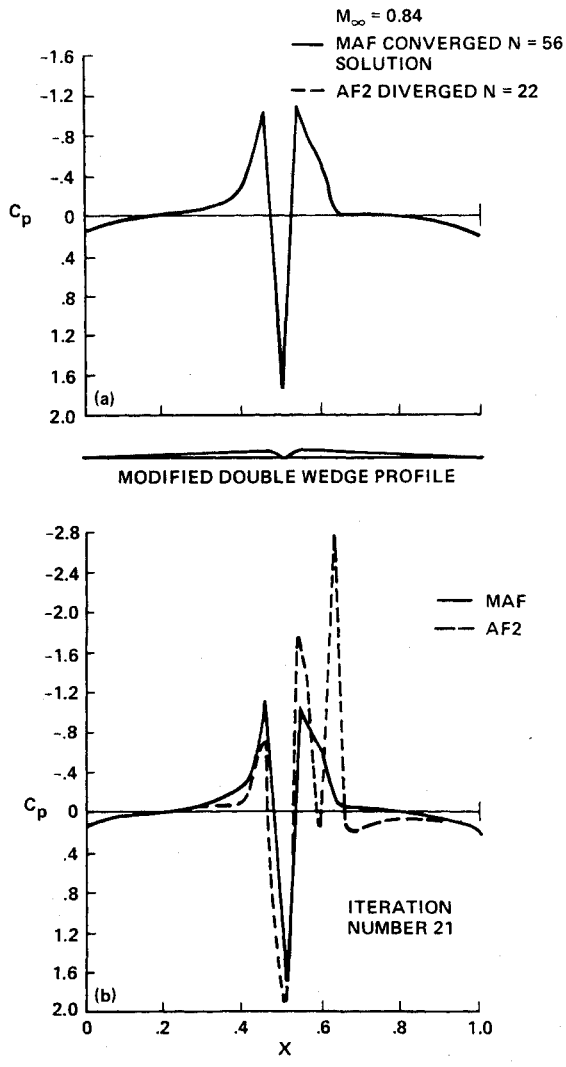


**Fig. 6 Comparison between monotone (MAF) and nonmonotone (AF2) algorithms for flow over a modified double-wedge profile: a) converged solution using MAF, nonmonotone algorithm diverged: b) iteration 21.**

histories. For this case, the AF2 code convergence had been previously optimized with $\alpha_H = 60$, $\alpha_L = 0.6$, $\omega = 2.0$, and CON = 1.5 $M^2_{i,j}$. This case demonstrates that this monotone switch is just as efficient as the highly efficient AF2 switch when the numerical instability in AF2 is not activated. The small-disturbance formula $C_p = -2(\phi_x - q_\infty)/q_\infty$ was used for these graphs.

The use of different forms of numerical dissipation can greatly affect the convergence rate of either MAF or AF2. For example, if the factor 1.5 is changed to 1.0 in the CON term, then $\alpha_H$ and $\alpha_L = 1$. With these values AF2 and MAF both take 655 iterations to converge. Initialy a monotone switch was tried that simply upwinded the flux components. Thus, instead of the flux in the supersonic region being given by Eq. (9) we tried

$$\tilde{\rho}_{i+\frac{1}{2},j}\delta_x\phi^n_{i,j} = \rho^*(u/q)^n_{i+\frac{1}{2},j} + [(\rho - \rho^*/q)u]^n_{i-\frac{1}{2},j}$$

instead. The best convergence rate for this dissipation was 1007 iterations when $\alpha_H = 333$ and $\alpha_L = 3.33$. This method of adding numerical dissipation was also developed independently by Boerstoel in Ref. 16.

In Eqs. (10) and (11), the test on $M_{i,j}$ may be ignored, so that $\tilde{\nu}$ and $\hat{\nu}$ are determined by tests only on $M_{i+\frac{1}{2},j}$ and $M_{i-\frac{1}{2},j}$. The calculations are again convergent in 125 iterations, but the shock profile is slightly smeared in comparison with the result shown in Fig. 4.

The second comparison is of a flow over an NACA 0012 airfoil at $M_\infty = 0.84$. In this case, the flow accelerated more severely over the leading edge; thus, the acceleration parameters had to be increased to $\alpha_H = 100$ and $\alpha_L = 1.0$ for both MAF and AF2 in order to obtain converged solutions. Both methods took 101 iterations to reduce the maximum residual by four orders of magnitude.

The third calculation is of flow over a double wedge profile with a dip in the middle, as illustrated in Fig. 6a. This profile was chosen to activate the numerical instability in the calculation using the AF2 method. This numerical instability occurs when the flow expands through the sonic value in proximity to a shock wave. Normally, this situation can occur in a lifting calculation, as shown in Fig. 3b for the small-disturbance equation. To simulate this situation for a nonlifting calculation, a modified double-wedge profile is used. Figure 6a shows the converged solution obtained by the MAF method. Convergence was obtained in 56 iterations, whereas the AF2 method developed a numerical instability and diverged in 22 iterations, as shown in Fig. 6b. The convergence criterion was the reduction of the maximum residual by four orders of magnitude. Both AF2 and MAF used $\alpha_H = 100$ and $\alpha_L = 1$.

### Conclusions and Remarks

By modifying the spatial differencing of AF2 algorithm[12] with a monotone method of adding numerical dissipation, a more stable scheme is formed, as shown by the calculation in Fig. 6. This modification required only minor coding changes in the research code used for these calculations. This monotone method can also be implemented in spatial differencing schemes that use general, i.e., non-Cartesian,[12,17,18] coordinate systems. For such systems the numerical dissipation should be added in th supersonic regions in the upwind directions along both coordinate lines. For unsteady calculations using the full potential equation,[18] we anticipate increases in allowable time-step sizes on the order of those demonstrated in Sec. III for the small-disturbance equation.

## Acknowledgment

We would like to thank Bram van Leer for explaining Godunov's method to us.

## References

[1]Harten, A., Hyman, J. M., and Lax, P. D., "On Finite Difference Approximations and Entropy Conditions for Shocks" *Communication on Pure and Applied Mathematics*, Vol. 29, 1976, pp. 297-322.

[2]Murman, E. M. and Cole, J. D., "Calculations of Plane Steady Transonic Flow," *AIAA Journal*, Vol. 9, Feb. 1971, pp. 114-121.

[3]Jameson, A., "Transonic Flow Calculations," VKI Lecture Series: Computational Fluid Dynamics, *Numerical Methods in Fluid Dynamics*, edited by H. J. Wirz and J. J. Smolderen, Hemisphere Publishing Co., 1978.

[4]Ballhaus, W. F., "A Fast Implicit Solution Procedure for Transonic Flows," Third International Symposium on Computing Methods in Applied Sciences and Engineering, Versailles, France, Dec. 1977.

[5]Ballhaus, W. F. and Goorjian, P. M., "Implicit Finite-Difference Computations of Unsteady Transonic Flows About Airfoils," *AIAA Journal*, Vol. 15, Dec. 1977, pp. 1728-1735.

[6]Godunov, S. K., "A Finite Difference Method for the Numerical Computation of Discontinuous Solutions of the Equations of Fluid Dynamics," *Mathematics of the USSR: Sbornik*, Vol. 47, 1959, pp. 271-290; also Cornell Aeronautical Lab. (Calspan) Translation.

[7]van Leer, B., "On the Relation Between the Upwind-Differencing Schemes of Godunov, Engquist-Osher and Roe," ICASE Rept. 81-11, March 1981.

[8]Goorjian, P. M., Meagher, M. E., and van Buskirk, R., "Montone Implicit Algorithms for the Small-Disturbance and Full Potential Equations Applied to Transonic Flows," AIAA Paper 83-0371, Jan. 1983.

[9]Goorjian, P. M. and van Buskirk, R., "Implicit Calculations of Transonic Flows Using Monotone Methods," AIAA Paper 81-0331, Jan. 1981.

[10]Engquist, B. and Osher, S., "Stable and Entropy Satisfying Approximations for Transonic Flow Calculations," *Mathematics of Computation*, Vol. 34, Jan. 1980, pp. 47-75.

[11]Jameson, A., "Transonic Potential Flow Calculations Using Conservative Form," *AIAA Second Computational Fluid Dynamics Conference Proceedings*, June 1975, pp. 148-161.

[12]Holst, T. L. and Ballhaus, W. F., "Fast, Conservative Scheme for the Full Potential Equation Applied to Transonic Flows," *AIAA Journal*, Vol. 17, Feb. 1979, pp. 145-152.

[13]Liepman, H. W. and Roshko, A., *Elements of Gasdynamics*, 6th ed., John Wiley and Sons, New York, 1965.

[14]Ballhaus, W. F. and Steger, J. L., "Implicit Approximate-Factorization Schemes for the Low-Frequency Transonic Equation," NASA TM X-73,082, Nov. 1975.

[15]Davis, S. S. and Malcolm, G. N., "Experimental Unsteady Aerodynamics of Conventional and Supercritical Airfoils," NASA TM-81221, 1980.

[16]Boerstoel, J. W., 'A Multi-Grid Algorithm for Steady Transonic Potential Flows Around Airfoils Using Newton Iteration," Symposium on Multigrid Methods, NASA CP-2202, Oct. 1981; also NLR MP 81050 U.

[17]Holst, T. L., "Implicit Algorithm for the Conservative Transonic Full-Potentital Equation Using and Arbitrary Mesh," *AIAA Journal*, Vol. 17, Oct. 1979, pp. 1038-1045.

[18]Goorjian, P. M., "Implicit Computations of Unsteady Transonic Flow Governed by the Full Potential Equation in Conservation Form," AIAA Paper 80-0150, Jan. 1980.